JOURNAL OF THEORETICAL AND APPLIED MECHANICS
52, 3, pp. 815-826, Warsaw 2014

BLADE COUPLE CONNECTED BY DAMPING ELEMENT WITH DRY FRICTION CONTACTS

Luděk Pešek, Ladislav Půst
Institute of Thermomechanics AS CR, Praha, Czech Republic
e-mail: pesek@it.cas.cz; pust@it.cas.cz

Theoretical and experimental solutions of forced vibration of a three-mass system linked together by two dry friction connections are presented. This system is a computational model of a physical model of a blade couple with a friction element measured in dynamic laboratory of Institute of Thermomechanics AS CR. Numerical solution of strongly nonlinear equations of motion shows good damping properties of the dry friction element and correspond to the results of experimental research, which is oriented on the investigation of both forced and free vibration of the physical blade couple model.

Keywords: dry friction, three masses system, damping of vibrations, irregular vibrations

1. Introduction

In order to quench unwanted and very dangerous vibrations of turbine bladed disks, various types of dampers are used, and large-scale research on this problem has been carried out in many institutes and laboratories in the world (Rao, 1991; Koh *et al.*, 2005; Ferrante *et al.*, 2012; Byrtus *et al.*, 2010). For the ascertaining of dynamic properties of bladed disks, a lot of theoretical, numerical and experimental studies have been done in Institute of Thermomechanics ASCR (e.g. Pešek and Půst, 2011a; Pešek *et al.*, 2012). The main focus of theoretical research is to elaborate basic background for diagnostic and identification methods for ascertaining the main properties of a real structure or an experimental model of turbine disks. The reduction of undesirable vibrations of blades is realized by using blade damping heads, which on the experimental model of turbine disk in the laboratories of the Institute of Thermomechanics (IT AS CR) are connected by inserted friction elements. For detailed examination of friction processes and their influence on blade vibrations, dynamic tests of a separated blade couple with the friction element have been performed (Pešek *et al.*, 2011; Půst and Pešek, 2012). Head tops of the blades are provided with friction surfaces creating a wedge-shaped inter-head slot. The friction element is pushed in the slot by the centrifugal force under rotation. For non-rotating tests, the static force F_c from the weight hanged on the string over the pulley substituted the centrifugal force.

Experimental laboratory research was completed by analytical and numerical solution of a simplified three degrees of freedom system, where the blades were modelled by one DOF slightly damped system connected by a friction element. The mentioned system, although very simple, contains two important dry friction connections, the properties of which have been intensively studied for a long time (e.g. Sextro, 2007; Awrejcewicz and Pyr'yev, 2009; Gallego and Nelias, 2007; Půst *et al.*, 2011). In order to prevent the friction element falling out of the slot during vibrations, either stops fixed to the friction element or auxiliary spring have to be used (Pešek and Půst, 2011b). Besides the dry friction damping, novelty approaches of passive vibration damping by means of piezoelectric actuators appear (e.g. Kozień and Kołtowski, 2011).

Simultaneously with the analytical solution of the investigated blade couple, laboratory measurements were carried out on the blade couple shown in Fig. 18. These experiments should

give the answer, among others, to the question how tangential stiffness in the contact surfaces changes the dynamic response of the entire system at very small vibrations, at so-called stick-slip motions.

2. Mathematical model of damping forces

For detailed examination of friction processes and their influence on blades vibrations, dynamic tests of the separated blade couple as well as tests of friction characteristics on s special experimental stand were performed. The behaviour of friction connection between the heads of blades has strongly nonlinear characteristic, where usually used Coulomb's model (Půst *et al.*, 2011) is given by

$$F_t = F_{t0}\,\mathrm{sgn}\,(v) \qquad \text{or} \qquad F_t = F_{t0}\frac{v}{|v|} \tag{2.1}$$

These expressions are only the first approximation of real properties. For a better description of the friction process, more sophisticated, e.g. modified, or stick-slip dry friction model has to be applied.

The further improvement is the "modified Coulomb friction" law expressed as a function of only one variable – relative velocity v. Contact micro-deformations are caused mostly by elastic deformations of bodies near the friction surfaces, but they are also accompanied by partial micro-slips in several points of the contact area, where owing to a non-uniform distribution of the contact pressure, a part of the area is less loaded.

The micro-slips at the very low velocity v can be therefore modeled by a linear increase of the friction force, as shown in Fig. 1a and Eqs. (2.2)

$$\begin{aligned} &F_t = F_{t0}\Big[\frac{v}{v_r}H(v_r - |v|) + \mathrm{sgn}\,(v)H(|v| - v_r)\Big] \qquad \text{or} \\ &F_t = kvH(v_r - |v|) + F_{t0}[\mathrm{sgn}\,(v)H(|v| - v_r)] \qquad \text{where} \qquad k = \frac{F_{t0}}{v_r} \end{aligned} \tag{2.2}$$

The critical velocity v_r is a velocity at which the micro-slip motion changes into full relative slip motion, F_{t0} is the Coulomb friction force proportional to the normal pressure $F_{t0} = fF_N$, H is the Heaviside function.

The discontinuity in the first derivative can sometimes evoke irregular oscillations and, therefore, it is possible to substitute this function by a continuous one – $\arctan\nu$.

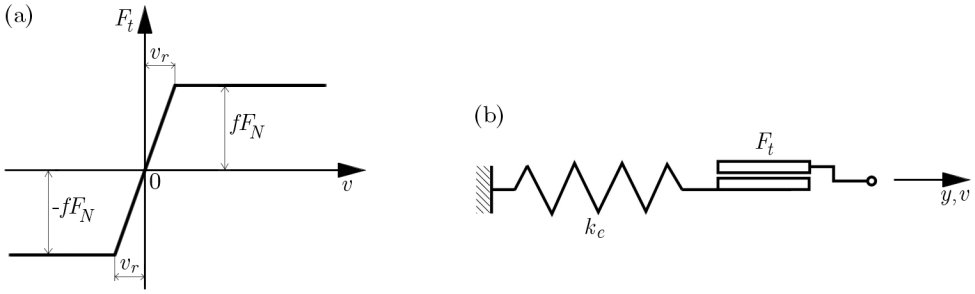

Fig. 1. (a) Modified Coulomb friction; (b) Stick-slip friction model

The more exact is the serial combination of Coulomb friction and spring stiffness (stick-slip model) drawn in Fig. 1b.

Its disadvantage is the dependence on two variables: velocity v and displacement y. The exact characteristic can be gained by integration. A rough mathematical model can be expressed by

$$\text{if} \quad |y| \leqslant \frac{F_{t0}}{k} \qquad \text{then} \qquad F_t = ky \qquad \text{else} \quad F_t = F_{t0}\,\mathrm{sgn}\,(v) \tag{2.3}$$

In the following analysis, the Coulomb dry friction law ($v_r = 0$) or modified Coulomb friction law ($v_r > 0$), or stick-slip models are used.

3. Simplified three-masses system

Experimental research gives important results useful for design and development of new machines, but it is usually encumbered with a lot of marginal influences and uncertainties. In this investigated case, it is e.g. very difficult to measure motion of the friction element, dry friction forces and friction coefficient during operation, etc.

Therefore, the additional analytical and numerical solution of the simplified mathematical model with exact parameters is very useful, and enables one to complete knowledge of the dynamic behaviour of studied system by the new information. Experimental system can be modelled by a simple three-mass system shown in Fig. 2, where the blades are replaced by 1 DOF systems. For simplicity, the excitation is supposed to be simply harmonic, acting on one blade.

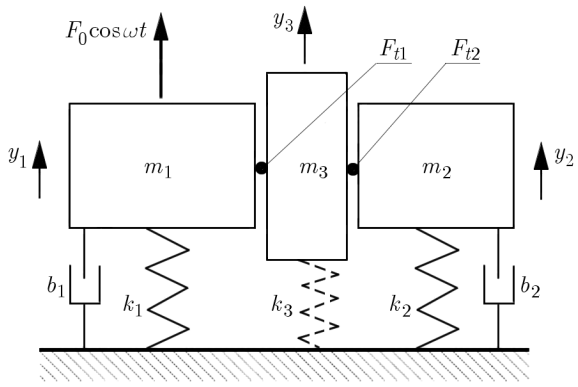

Fig. 2. Mathematical 3DOF model

Damping of both blades is in Fig. 2 modelled by small viscous damping with coefficients $b_1 = b_2 = 0.1\,\mathrm{Ns/m}$. For elimination of the gravitational force, the friction element $m_3 = 0.01\,\mathrm{kg}$ was hanged on a very weak spring with stiffness $k_3 = 1000\,\mathrm{N/m}$. The differential equations of motion are then

$$\begin{aligned} &m_1\ddot{y}_1 + b_1\dot{y}_1 + k_1 y_1 + g_1(y_1 - y_3, \dot{y}_1 - \dot{y}_3) = F_0\cos\omega t \\ &m_2\ddot{y}_2 + b_2\dot{y}_2 + k_2 y_2 + g_2(y_2 - y_3, \dot{y}_2 - \dot{y}_3) = 0 \\ &m_3\ddot{y}_3 + k_3 y_3 + g_1(y_1 - y_3, \dot{y}_1 - \dot{y}_3) - g_2(y_2 - y_3, \dot{y}_2 - \dot{y}_3) = 0 \end{aligned} \tag{3.1}$$

where the excitation frequency of the force $F_0\cos\omega t$ varies near to the eigenfrequencies of the main subsystems

$$\omega \approx \sqrt{\frac{k_1}{m_1}} = \sqrt{\frac{k_2}{m_2}}$$

The nonlinear functions g_1, g_2 consist of linear elastic forces modelling the tangential stiffness in the contact surfaces (stick deformation) and nonlinear Coulomb's dry friction damping forces (slip motion). Mathematically, they can be described by some of expressions (2.1)-(2.3).

Motion of the investigated system is further solved by direct numerical solution of equations (3.1), with using the Runge-Kutta integration methods in Matlab Language.

4. Examples of motions

4.1. System with Coulomb friction contacts

If we suppose, that the friction element has no stops and no tangential deformation in the contact surfaces (stick deformation) exists, then only Coulomb's dry friction, Eq. (2.1), connects the three-mass system. This system was solved in Pešek and Půst (2011b); from there we present here only selected results. For the equal main systems $m_1 = m_2 = 0.182\,\mathrm{kg}$, $k_1 = k_2 = 105000\,\mathrm{kgs}^{-2}$, the amplitude of the exciting force $F_0 = 1\,\mathrm{N}$, damping force $F_{t0} = 0.35\,\mathrm{N}$ and stiffness of the supporting spring $k_3 = 1000\,\mathrm{N/m}$ the amplitude response curves $a_1(f)$, $a_2(f)$, $a_3(f)$ are calculated and shown in Fig 3a. Motion a_3 of the friction element m_3 contains small but visible chaotic components, which are also contained, however in a smaller rate, in motions a_1, a_2 of much greater masses m_1 and m_2. The response curves $a_2(f)$ and $a_3(f)$ meet at the excitation frequency $f = 119.9\,\mathrm{Hz}$ and they run together in a higher frequency range. This change of motion is manifested itself also by a small break in the response curve $a_1(f)$ at $f = 119.9\,\mathrm{Hz}$.

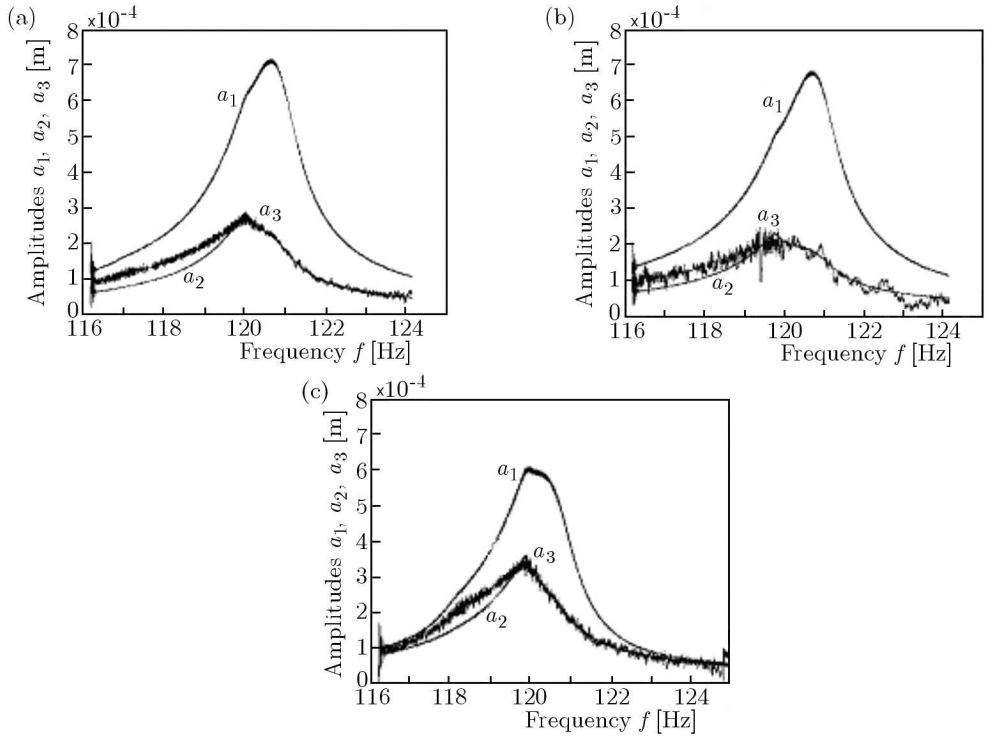

Fig. 3. Response curves: (a) $F_{t0} = 0.35\,\mathrm{N}$, $k_3 = 1000\,\mathrm{N/m}$; (b) $F_{t0} = 0.5\,\mathrm{N}$, $k_3 = 100\,\mathrm{N/m}$; (c) $F_{t0} = 0.5\,\mathrm{N}$, $k_3 = 1000\,\mathrm{N/3}$

In Fig. 3b, the response curves $a_1(f)$, $a_2(f)$, $a_3(f)$ are shown for the same parameters as in the previous figure, but for 10 times lower stiffness $k_3 = 100\,\mathrm{N/m}$ of the spring supporting the inserted friction mass m_3. It is shown that the irregular components of $x_3(t)$ motion increase, but the global form of all averaged response curves does not change essentially.

An increase in the damping force from $F_{t0} = 0.35\,\mathrm{N}$ up to $F_{t0} = 0.5\,\mathrm{N}$ brought down the resonance peaks. The response curves for $k_3 = 1000\,\mathrm{N/m}$ are shown in Fig. 3c. In comparison with Fig. 3a ($F_{t0} = 0.35\,\mathrm{N}$), the maximum amplitude a_1 decreases, a_2 increases and after a break of $a_1(f)$ at $f = 119.9\,\mathrm{Hz}$ both response curves $a_1(f)$ and $a_2(f)$ sink continuously.

The response curves of the system containing Coulomb dry friction elements contain some breaks, caused by the sudden changes of system properties, when the stiff friction connections between the main masses and friction elements jump into slip motion. No such a phenomenon

has been observed during the laboratory experiments on the physical models of bladed bundles, which indicates that the sudden jump of the friction force at the velocity reversal passes more continuously. Therefore, the modified Coulomb dry friction law can give a true picture of the friction force processes near the dwell points of vibrations.

4.2. System with modified Coulomb friction contacts

In order to approximate the numerical results to real behaviour of the blade couple, let us solve the response curves of the investigated blade couple by application of friction connections described by the modified Coulomb friction law expressed in Eq. (2.2) and Fig. 1a. The parameters of this contact as well as other physical quantities for the numerical solution are used the same as in the laboratory measurements (Section 6).

The response curves of the blade couple connected by a steel friction element and the friction connections with the neighbouring blades are modelled by the modified Coulomb dry friction according to Fig. 1a and are shown in Fig. 4a for $F_{t0} = 0.4\,\mathrm{N}$. It is evident that for a low dry friction force $F_{t0} = 0.4\,\mathrm{N}$, the discontinuity in the first derivative evokes strong irregular oscillations which can be removed either by introducing additional damping or by smoothening the dry friction characteristics.

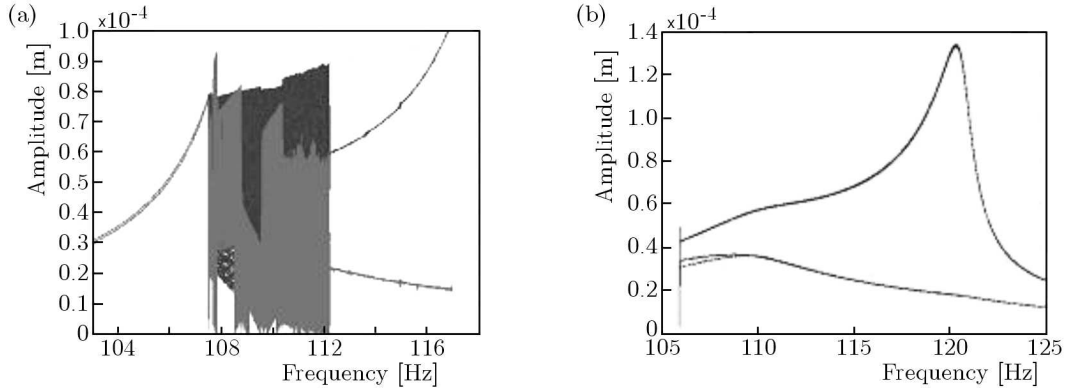

Fig. 4. Response curves at low dry friction force: (a) modified Coulomb dry friction; (b) smooth arcus-tangens characteristic

After replacing the broken dry friction characteristic by the smooth arcus-tangens function, the irregular oscillations disappear and the curves have continuous courses as shown in Fig. 4b.

The upper response curve $a_1(f)$ in the last figure reaches a high resonance peak at the frequency $f = 120.2\,\mathrm{Hz}$ corresponding to the eigenfrequency of the excited blade. A similar start of this resonance is seen also in Fig. 4a. The resonance of the blade couple when both blades and friction elements are sufficiently connected by the friction forces lies at $f = 110\,\mathrm{Hz}$, and it is only very weakly indicated in Fig. 4b. The motions of the second unexcited blade and of the friction element getting connected together at $110\,\mathrm{Hz}$ continue to move together as a one subsystem with descending amplitudes at higher frequencies. However, due to the high resonance peak of the first excited blade, it is evident that the friction force $F_{t0} = 0.4\,\mathrm{N}$ is insufficient for the correct function of the inserted dry friction element.

An increase in the dry friction force up to the value $F_{t0} = 0.6\,\mathrm{N}$ changes markedly the picture, as shown in Fig. 5a. The separate resonance peak of $a_1(f)$ at $f = 120.2\,\mathrm{Hz}$ disappears, all three response curves become close together, and only the resonance peaks at $f = 110\,\mathrm{Hz}$ exist. In comparison to the previous case, the amplitudes of all masses at this frequency are higher.

A further increase in the dry friction force up to the value $F_{t0} = 0.8\,\mathrm{N}$ (Fig. 5b) causes both the rapprochement of all curves and an increase of resonance peaks. All masses vibrate connected in frequency range over $f = 118\,\mathrm{Hz}$.

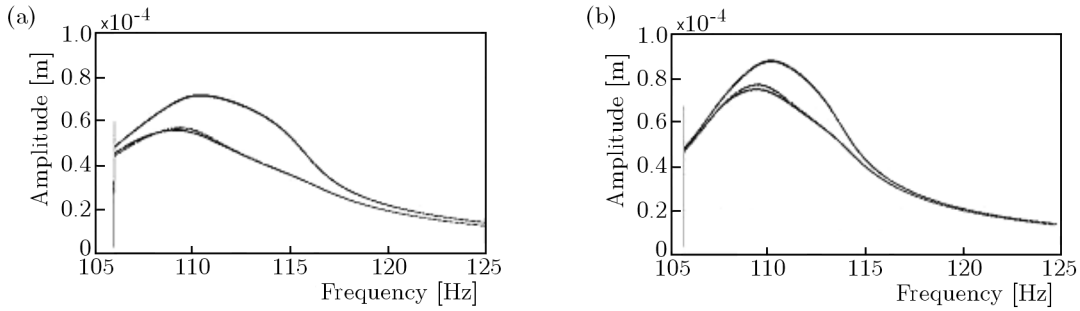

Fig. 5. Dry friction force $F_{t0} = 0.6\,\mathrm{N}$ (a) and $F_{t0} = 0.8\,\mathrm{N}$ (b), arcus-tangens characteristic

From these several selected examples, we can decide that the dry friction forces in the contact surfaces of the friction element have the optimum (approx. $F_{t0} = 0.5\,\mathrm{N}$). The damping effect at lower or higher dry friction forces is always worse.

5. Computational modelling of free vibration amplitude decay

Damping properties of the investigated system can be evaluated also from the vibration amplitude decay of blades which are excited into the resonance state when the forced mode of vibration is very near to the eigenmode and then this excitation is sudden switched-off. Damping ratios are identified from the logarithmic decrement of the amplitude decay. The qualitative analysis is sometimes sufficient for the information of damping properties with variable amplitudes.

Because experiments carried out in laboratory IT ASCR have been oriented also on the application of special composite material ARAMID, having good friction properties, wear and heat resistance for the damping material e.g. in LP steam turbines, theoretical analysis of this system has been realized as well.

Friction elements made of ARAMID are more compliant in comparison with steel, which plays important role at small amplitude vibration. Therefore, the slip-stick model of the friction characteristic has to be used.

Mass of the friction element is $m_3 = 0.01\,\mathrm{kg}$ and its slip-stick characteristic has rheologic parameters: $F_{t0} = 1.25\,\mathrm{N}$, $k_1 = 30000\,\mathrm{N/m}$. Numerical results of the amplitude decays for both blade masses are shown in Fig. 6a.

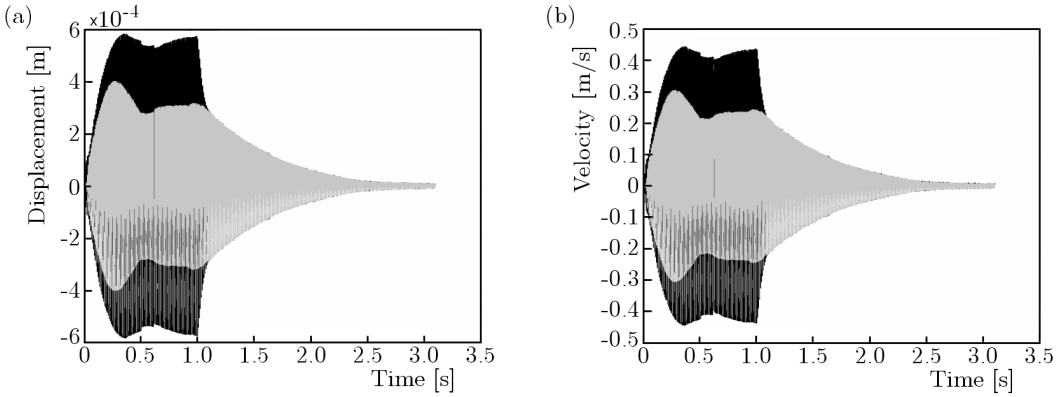

Fig. 6. Slip-stick characteristic: (a) displacement-time, (b) velocity-time

The quick first part of the decay corresponds to high damping caused by the energy loss at dry friction slip, the envelope break indicates the end of the slip period and the beginning of

the stick period when no friction losses exist and only losses of deformation energy in the blades and element material influence the decay.

The record of velocity of the same process is shown in Fig. 6b. Because the motions are purely harmonic and recorded at the constant frequency, both figures are qualitative the same, the only difference is in the vertical scales.

The detailed analysis of reverberation processes is better to realize from the records of envelope curves where all three dependencies can be clearly seen. The influence of individual parameters of the stick-slip characteristic (spring stiffness k_1, dry friction force F_t) on the entire process can be investigated.

The effect of the magnitude of dry friction force F_t at a constant value of spring stiffness $k_1 = 50000\,\mathrm{N/m}$ is seen from comparison of Fig. 7.

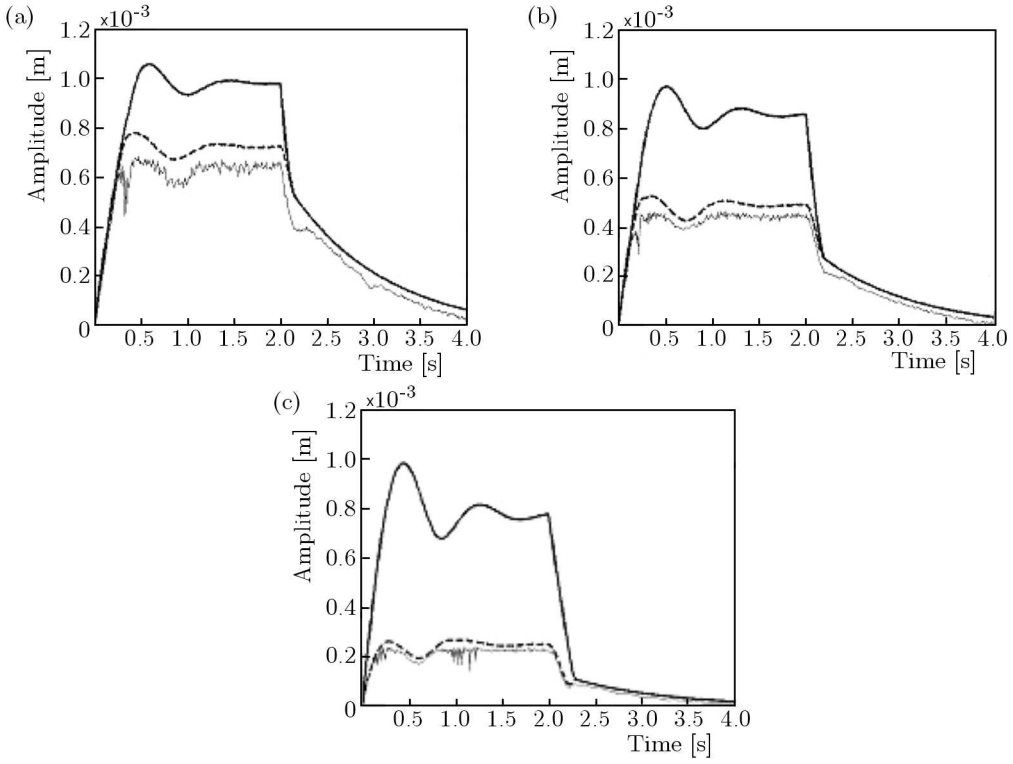

Fig. 7. Friction force: (a) $F_t = 1.5\,\mathrm{N}$, (b) $F_t = 1\,\mathrm{N}$, (c) $F_t = 0.5\,\mathrm{N}$

The amplitudes a_1 of the excited mass m_1 during the excitation period (time 0-2 s) decrease very weakly with decrease in the friction force $F_t = 1.5,\ 1,\ 0.5\,\mathrm{N}$, as seen from the highest full curves. However, the amplitudes a_2 of the non-excited mass m_2 (dashed curve) during the excitation period decreases proportionally to the friction force. Differences between both these curves increase. Motion of the inserted friction element copy approximately the motion of mass m_2, but its motion is mildly distorted by a random signal.

Sudden jumps of all amplitudes occur at the switch-off of the excitation force (period 2-4 s). The height of jumps of the amplitude a_1 slightly increases with a decrease in the friction force. The jumps of the amplitude a_2 have roughly the same height. After the jump, all three masses join together, and the mild decrease follow. Amplitudes of this reverberation process are high at high friction forces and decrease more than proportionally with the decreasing friction force.

Similar analysis can be done also on the influence of stick stiffness k_1. The decrease of the stick stiffness $k_1 = 50000\,\mathrm{N/m}$ (weak curves in Fig. 8a) on the tenth value $k_1 = 5000\,\mathrm{N/m}$ (full curves) at the friction force $F_t = 1.5\,\mathrm{N}$ causes comparatively small shifts of the blade

amplitudes a_1, a_2, but the motion of the friction elements is more sensitive to the lowering of contact stiffness.

The blade bundle properties presented in Fig. 8a can be generalized only with great caution, as the investigated system containing two strongly nonlinear connections is for prediction of an exact dynamic behavior dangerous case. An example of such another property is given in Fig. 8b, where the same jump in the contact stiffness $k_1 = 50000\,\mathrm{N/m}$ on the tenth value $k_1 = 5000\,\mathrm{N/m}$ for a small friction force $F_t = 0.5\,\mathrm{N}$ has practically no influence on the courses of envelopes of both blade amplitudes. The only changes are seen in motion of the dry friction element.

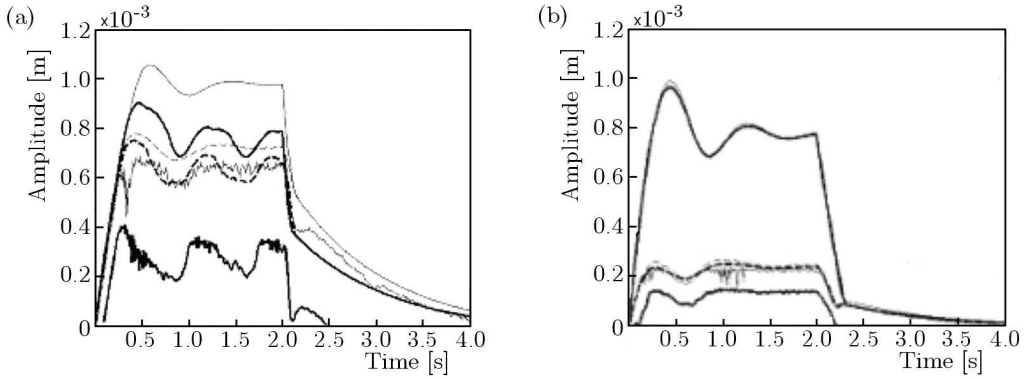

Fig. 8. Responses at $k_1 = 5000\,\mathrm{N/m}$ (bold), $k_1 = 50000\,\mathrm{N/m}$ (thin): (a) $F_t = 1.5\,\mathrm{N}$, (b) $F_t = 0.5\,\mathrm{N}$

By means of several examples, it has been shown that the serial combination of Coulomb friction and spring stiffness (slip-stick model) can be successfully applied for computational modeling of vibration amplitude decay processes that are used for evaluation of damping properties of experimentally investigated dynamic systems. The comparison of time histories gained experimentally with the numerical solution enables one to ascertain the friction and contact stiffness characteristics.

6. Experimental investigation of the blade couple with the damping element

For the evaluation of the element influence on the blade vibration damping, experiments of the blade couple with the friction element made of steel or composite material ARAMID were performed in the steady non-rotating state (Fig. 9). Blades A and B (prismatic part: width $\times$ thickness $0.02 \times 0.01\,\mathrm{m}$, length $0.2\,\mathrm{m}$, total length $0.25\,\mathrm{m}$) were clamped in the lower ends into the steel block by bolts (Fig. 9). The friction element (FE) placed in the slot between the blade ends (height $0.01\,\mathrm{m}$, mass $0.078\,\mathrm{kg}$) was radially extruded by the thread prestressed by the static force F_r. The radial force was set in the range up to $5\,\mathrm{N}$.

The dynamic force acting on blade A was either an eletrodynamic or electromagnetic force. For description of the damping effect of dry friction contacts, the excitation and damping evaluations were performed by two different scenarios:

S1) a short block (several seconds in length) of harmonic excitation with the first resonant flexural frequency of the blade fixed on the disk for different static radial F_r and excitation amplitude F_a; the damping effect was evaluated from the vibration amplitude decay of blades after abrupt switching-off the excitation; damping ratios were identified from the amplitude logarithmic decrement by Hilbert's transformation.

S2) very slow sweep frequency excitation in the range covering the first resonant flexural frequency of the blade fixed on the disk for different static radial forces F_r; the maximal amplitude frequency functions (MAF) were obtained by the ratio of maximal amplitudes of the force and response time signals. The damping effect was evaluated from the

frequency response functions (FRF) obtained by FFT analysis with the averaging of the force/response signals. The eigenvalues of the flexural blade vibration were identified by the fitting algorithm Least Squares Frequency Domain (LSFD).

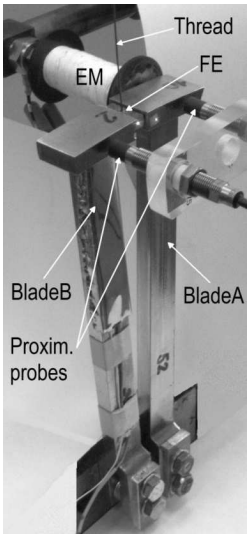

Fig. 9. Picture of the measurement set-up (small light spots – target laser points)

Each blade displacement u_A responses u_B was picked up by proximity probes Schenk IN-081, and at the same time velocities v_A of blade A and v_{FE} of the friction element by POLYTEC laser vibrometers were measurement. Electromagnet EM or shaker LDS-V406 was supplied by LDS power amplifier and controlled by a signal of generator HP 33120A. The dynamic force was measured by force transducer B&K8200. Time characteristics of the force, blade and friction element responses, generator signals were registered in Scope Recorder YOKOGAWA DL750.

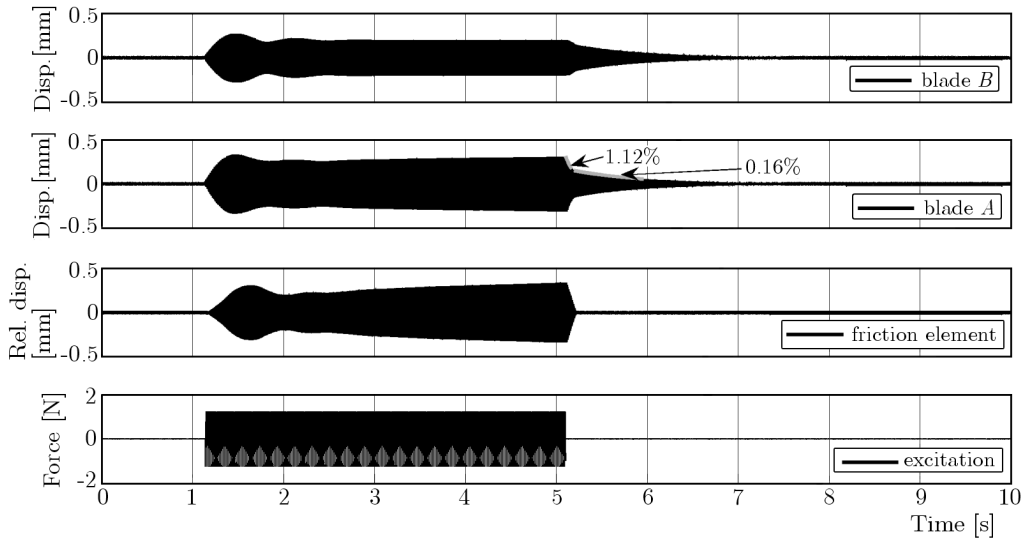

Fig. 10. Graphs of the blade couple responses, i.e. displacements of blade B and A, relative displacement of the friction element and electromagnet force – ARAMID FE, static radial force 0.5 N, excitation amplitude 1.6 N. Grey lines depict the amplitude envelope during the attenuation phases of blade A vibration

A typical result of the two blades vibration with the ARAMID friction element obtained by scenario $S1$ is shown in Fig. 10 for the radial force $F_r = 0.5$ N and excitation amplitude

$F_a = 1.6\,\mathrm{N}$. The top graphs of the figure depict the measured signals, i.e. displacements of blades A, B, relative displacement of the friction element with respect to blade A and electromagnet force F_{em}. The relative displacement was evaluated from the difference of velocities v_A and v_{FE} after their integrations. The second graph in Fig. 10 shows additionally the displacement of blade A and evaluated damping ratios at vibration attenuation phases after switch-off of the electromagnet current supply.

The non-linear effect of dry friction is mostly pronounced in attenuation phase (5.1 s) where macro-slips occur between blade A and the friction element as the relative displacement of the friction element shows (Fig. 10). Due to macro-slips, the vibration amplitudes of blade A fall down with a high damping ratio of 1.12%. After this phase, the macro-slips movement transfers into the micro-slip-stick contact movements of the friction element, and the blades and the damping ratio drop down to 0.16%.

Typical results of the maximal amplitude frequency (MAF) function of both blades with the steel friction element obtained by scenario $S2$ for the static radial force $F_r = 0.5\,\mathrm{N}$, 1 N and 0.2 N, and the excitation amplitude $F_a = 0.8\,\mathrm{N}$ are shown in Figs. 11a, 11b and 11c, respectively. For values of F_r under 0.5 N, the movement of the friction element becomes pronounced in the inter-head space and only the additional axial stops prevent from the extrusion of the element from the slot. In spite of higher macroslips of the friction element with respect to higher F_r occurred in the slot, the maximal amplitudes of blades vibration rose (Fig. 11c). It is caused both by smaller friction contact forces and the side effect of impacts of the stops of the friction element with the blades.

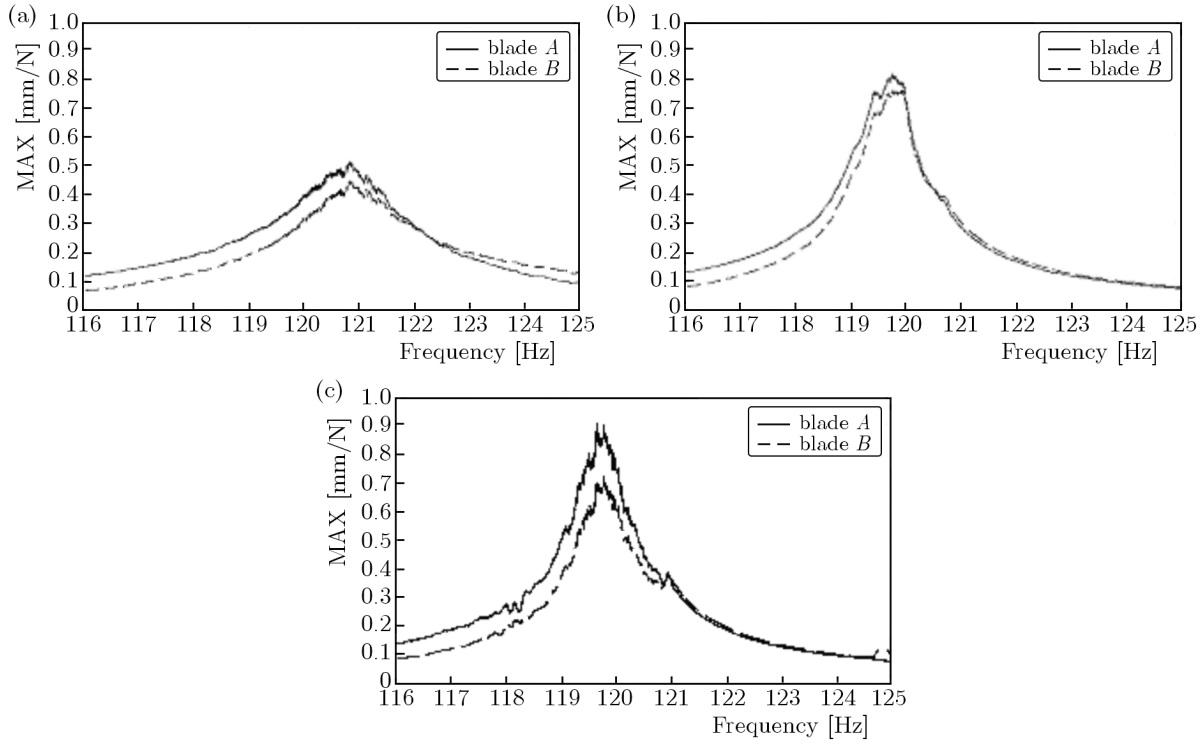

Fig. 11. Maximal amplitude frequency functions of the blade couple linked by the friction element evaluated from the sweep excitation – steel FE, excitation amplitude 0.8 N and static radial force: (a) 0.5 N, (b) 1 N, (c) 0.2 N

The damping ratio dependence on the force F_r ($\geqslant 0.5\,\mathrm{N}$) is evaluated in Fig. 12. This graph clearly shows that the damping rises with decreasing values of F_r due to higher macro-slips in the contact surfaces.

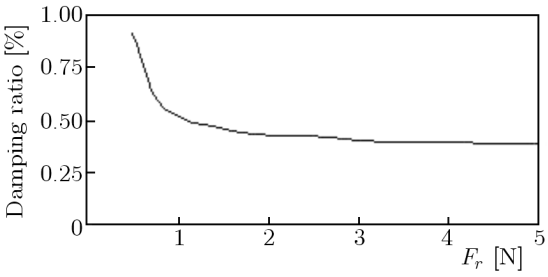

Fig. 12. Dependence of the damping ratio on the radial force

7. Conclusion

Analysis of dynamic behaviour of numerical and experimental models of the blade couple with an inserted dry-friction damping element is presented. The experimental results were used for parameter estimation and validation of the numerical contact models.

The elaborated method of numerical solution and obtained results create a basic theoretical background for the evaluation of measurement on a laboratory experimental bladed disk set and for the evaluation of effectiveness of the friction element on suppression of forced vibration of the blades. It was shown that its suppression of undesirable resonance vibrations depends also on the magnitude and type of dry friction characteristic. Original Coulomb's dry friction characteristic, modified (micro-slip) and stick-slip models were used in the paper, but more sophisticated friction models can be applied as well.

Strong nonlinear discontinuity of dry friction near zero velocity excited by the sudden jump of the friction force $\pm F_{t0}$ caused irregular vibrations, but this irregular behavior can be simply removed by introducing either small damping into displacement or suppressed by micro-slips in reverse velocity points.

The experimental investigations showed the dependence of the damping ratio of the blade couple on the radial prestress of the friction element in the inter-blade slot for a given value of the amplitude of the excitation force. The damping rises with decreasing values of the radial prestress due to higher macro-slips in the contact surfaces. It is, however, valid only up to a certain value of the prestress, then the contact friction forces become weak and dissipation of the vibration energy diminishes. The numerical results using the modified Coulomb dry friction characteristic are in agreement with the experiment.

The non-linear damping effect of the friction couplings in the blade couple was studied from the free vibration attenuation, too. The higher damping appears when the macro-slips appear in the friction contacts at higher blade displacements. When the displacements decrease, the macro-slips transmit into the microslip movement and the magnitude of damping decreases rapidly. It was proven that the stick-slip numerical model of the contact is appropriate for description of this behaviour.

Acknowledgement

This work was supported by the research project of the Czech Science Foundation No. 101/09/1166 "Research of dynamic behavior and optimization of complex rotating system with non-linear couplings and high damping materials", and by the research institutional fund RVO: 613889.

References

1. Awrejcewicz J., Pyr'yev Yu., 2009, *Nonsmooth Dynamics of Contaction Thermoelastic Bodies*, Springer Verlag
2. Byrtus M., Hajžman M., Zeman V., 2010, *Dynamics of Rotating System* (in Czech), University of West Bohemia, Pilsen

3. Ferrante M., Pesatori E., Bachschmid N., 2012, Simulation of the dynamic behaviour of a group of blades with friction contacts, *10th International Conference on Vibrations in Rotating Machinery*, 189-198, ISBN 978-0-85709-452-0

4. Gallego L., Nelias D., 2007, Modelling of fretting wear under gross slip and partial slip conditions, *Journal of Tribology*, **129**, 3, 528-536

5. Koh K.H., Griffin J.H., Filippi S., Akay A., 2005, Characterization of turbine blade friction dampers, *Transaction of the ASME*, **127**, 856-862

6. Kozień M.S., Kołtowski B., 2011, Comparison of active and passive damping of plate vibration by piezoelectric actuators – FEM simulation, *Acta Physica Polonica A*, **119**, 6-A, 1005-1008

7. Pešek L., Půst L., 2011a, Influence of dry friction damping on bladed disk vibration, *Vibration Problems ICOVP 2011*, Náprstek J., Horáček J. (Edit.), Berlin, Springer, 557-564

8. Pešek L., Půst L., 2011b, Mathematical model of a blade couple connected by damping element, *Proceedings of the 8th International Conference on Structural Dynamics, EURODYN2011*, Leuven, Katolieke Universiteit Leuven, 2006-2011

9. Pešek L., Půst L., Bula V., Vaněk F., Cibulka J., 2012, Inter-slip damping of twisted blades in opposed bundles under rotation, *10th International Conference on Vibrations in Rotating Machinery*, 293-302, ISBN 978-0-85709-452-0

10. Pešek L., Půst L., Vaněk F., Veselý J., 2011, FE Modeling of blade couple with friction contacts under dynamic loading, *Proceedings of the 13t World Congress in Mechanism and Machine Science (IFToMM 2011)*, Guanajuato, Mexico, 1-8

11. Půst L., Pešek L., 2012, Mathematical model of two blades system, *Vibration Engineering and Technology of Machinery VETOMAC 8*, Szewalski Institute of Fluid-Flow Machinery, PAS, Gdańsk, 199-208, ISBN 978-83-88237-61-4

12. Půst L., Pešek L., Radolfová A., 2011, Various types of dry friction characteristics for vibration damping, *Engineering Mechanics*, **18**, 3/4, 203-224, ISSN 1802-1484

13. Rao, J.S., 1991, *Turbomachine Blade Vibration*, Wiley Eastern Limited

14. Sextro, W., 2007, *Dynamical Contact Problems with Friction*, Springer-Verlag, 2nd edition

Manuscript received November 29, 2013; accepted for print March 4, 2014